

Architecture for fast implementation of qLDPC codes with optimized Rydberg gates

C. Poole,¹ T. M. Graham,¹ M. A. Perlin,² M. Otten,¹ and M. Saffman^{1,3}

¹*Department of Physics, University of Wisconsin-Madison, 1150 University Avenue, Madison, WI, 53706 USA*

²*Inflection, Inc., Chicago, IL, 60615, USA*

³*Inflection, Inc., Madison, WI, 53703, USA*

(Dated: April 30, 2024)

We propose an implementation of bivariate bicycle codes (Nature **627**, 778 (2024)) based on long-range Rydberg gates between stationary neutral atom qubits. An optimized layout of data and ancilla qubits reduces the maximum Euclidean communication distance needed for non-local parity check operators. An optimized Rydberg gate pulse design enables CZ entangling operations with fidelity $\mathcal{F} > 0.999$ at a distance greater than $12 \mu\text{m}$. The combination of optimized layout and gate design leads to a quantum error correction cycle time of $\sim 1.2 \text{ ms}$ for a $[[144, 12, 12]]$ code, an order of magnitude improvement over previous designs.

Recently, a new family of quantum low density parity check (qLDPC) codes known as quasi-cyclic “bivariate bicycle” codes was proposed and analyzed in Ref. [1]. These bicycle codes were found to have encoding rates greatly exceeding that of the surface code [2], pseudothresholds competitive with the surface code, and a Tanner graph with “thickness” 2. As pointed out in Ref. [1], the thickness-2 Tanner graph motivates a qubit layout on a dual-sided superconducting chip. The bicycle codes have weight-6 check operators whose measurement requires long-distance interactions. The need to incorporate long-distance connections is intrinsic to any code that improves on the density of stored quantum information compared to the surface code, which saturates the BPT bound found in Ref. [3].

It has been proposed [4] to implement the non-local connectivity required for bivariate bicycle codes with neutral atom qubits using atom-transport techniques [5]. While transport provides long-range connectivity, it is also intrinsically limited in speed [6], and quantum error correction (QEC) cycle times for measuring a full set of X and Z parity checks were estimated to be $\sim 10 \text{ ms}$. An implementation of hypergraph qLDPC codes based on atom transport also leads to QEC cycle times of tens of milliseconds [7]. This slow cycle time calls into question the utility of these implementations for applications that require deep circuits or large numbers of samples [8].

We propose here to use a neutral atom architecture based on fast optical beam scanning [9] that incorporates two innovations to reduce the QEC cycle time by more than an order of magnitude compared to transport-based approaches. Our first contribution, illustrated in Fig. 1, is the introduction of a qubit layout that can reduce the largest Euclidean communication distance that is required to perform parity check operations by almost a factor of 3 relative to known layouts [1, 4]. The second contribution is an optimized Rydberg gate design that minimizes the required two-atom interaction strength while maintaining fast speed and high fidelity. Together, these approaches make it feasible to implement high performance bicycle codes up to distance $d = 18$ without

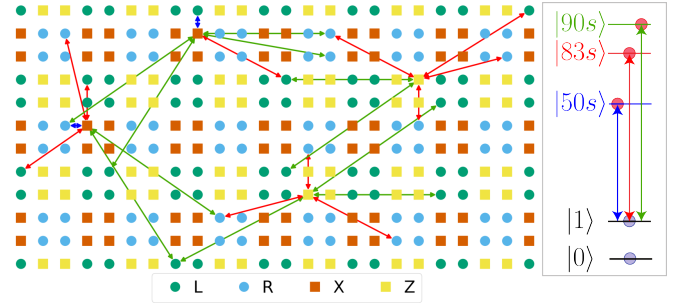


FIG. 1. Optimized layout of the $[[144,12,12]]$ code with a maximum communication distance of 7.21 lattice spacings. The check operations are shown for a few ancilla qubits with color coded connections corresponding to the Cs Rydberg levels shown on the right. The qubit color coding is L data = green circle, R data = blue circle, X check = red square, Z check = yellow square.

relying on atom transport. The estimated QEC cycle times, assuming fast qubit measurements, are $\sim 1.2 \text{ ms}$, which is an order of magnitude improvement over existing proposals. We address the issue of achieving fast qubit measurement time at the end of this letter.

Table I provides, for several bivariate bicycle codes with code distances $d = 6-18$, the maximum communication distance D_{max} required to implement these codes when qubits are laid out on a rectangular grid as described in Ref. [1] and [4], as well as the required D_{max} when following a qubit assignment procedure that we describe below. For several of the codes, including the $[[144, 12, 12]]$ code that we will examine in more detail, the maximum distance arises from the check operation which would be nearest neighbor on a torus, but stretches from one side of the qubit grid to the other for a planar layout with open boundary conditions, as in Fig. 2a.

Rydberg gates for neutral atom qubits require an atom spacing that is at least the diameter of the Rydberg wavefunction in order to avoid collisions between Rydberg electrons, or between a Rydberg electron and a neighboring atomic core. This limit is about $1 \mu\text{m}$, which is the wavefunction diameter for a Rydberg atom in a low an-

TABLE I. Bivariate bicycle codes with n data qubits, $2n$ total qubits (including ancillae), k logical qubits, and code distance d . The figure of merit $r = kd^2/n$ quantifies an improvement over the (rotated) surface code for which $r = 1$ with any choice of k or d . For each code, we report the maximum communication distance D_{\max} in units of the lattice spacing using the qubit layouts in Refs. [1, 4], and with optimized layouts found in this work (see main text for explanation).

code	f.o.m.	IBM [1]	UC [4]	this work
$[[n, k, d]]$	r	D_{\max}	D_{\max}	D_{\max}
$[[72, 12, 6]]$	6.	11.	11.	5.
$[[90, 8, 10]]$	8.89	29.	25.	10.
$[[108, 8, 10]]$	7.41	17.	15.	7.
$[[144, 12, 12]]$	12.	23.	21.	7.21
$[[288, 12, 18]]$	13.5	27.7	21.	7.21

gular momentum state with principal quantum number $n = 100$. There are also practical limits to how tightly the laser beams used for Rydberg excitation can be focused without crosstalk arising from tails of the optical beam profiles. A feasible, albeit demanding, practical limit is an atom separation of at least $s_{\min} \simeq 1.5 \mu\text{m}$. A high fidelity Rydberg CZ gate requires at least a few MHz of interaction strength [10], and this limits the physical interaction distance to $R_{\max} = 10 - 15 \mu\text{m}$, or about $10s_{\min}$. We see that the layouts given in Refs. [1, 4] only approach this limit for the $[[72, 12, 6]]$ code, but have substantially longer communication distances for the higher performance codes.

In order to implement check operations without atom transport the communication distance, or the requirement on Rydberg interaction strength, needs to be reduced. We proceed to show how both parameters can be improved. To reduce the communication distance we change the layout of the qubits in a planar rectangular grid, as in Fig. 1. We proceed by placing each of the L and R data qubits in the plane following an enumeration scheme which is a generalization of the method used in [1], but which is not restricted by the requirement that there are four nearest neighbor check operators for each qubit under periodic boundary conditions. Details are given in [11]. The entire grid is then remapped according to the “folding” procedure illustrated in Fig. 2. At this stage, the positions of L and R qubits are considered fixed, and we then identify an assignment of X and Z qubits which minimizes the maximum check operator distance D_{\max} .

To identify whether or not it is possible to find a mapping such that the distance of all check operators is $D \leq D_{\max}$, we define an interest matrix \mathbf{I} where $\mathbf{I}_{ij} = 1$ if ancilla qubit i when placed in lattice site j has distance $D \leq D_{\max}$ for every check operator involving i , and 0 otherwise. In this way, the rows and columns of \mathbf{I} represent two partitions of a bipartite graph. If the graph admits

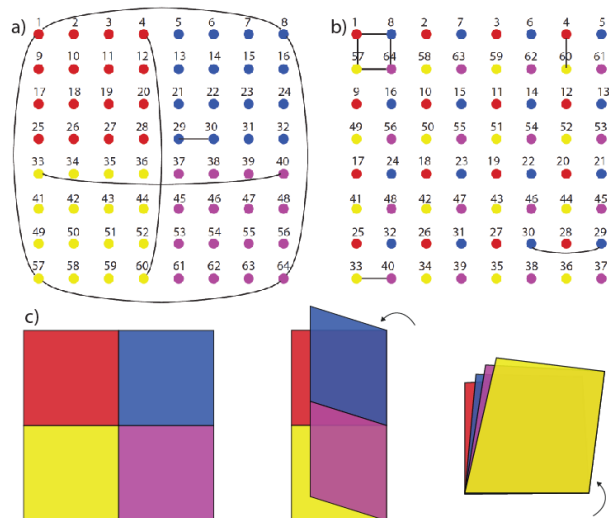


FIG. 2. a) A grid of nearest-neighbor connected qubits on a torus has long range connections when mapped onto a planar grid with open boundary connections. b) A remapping procedure converts long-range connections into nearest-neighbors, and neighboring connections into nearest- or next-nearest neighbors [12]. c) This remapping is achieved by “folding” the plane in a) once vertically and again horizontally and expanding each quadruplet of overlapping qubits into a square as in panel b). Only a few connections are shown for clarity.

a perfect matching, then the matching provides a placement satisfying the distance constraint for all check operators. To find the minimum satisfiable D_{\max} , we enumerate all possible values of $D_{\max}(\delta x, \delta y) = \sqrt{\delta x^2 + \delta y^2}$ and test progressively more restrictive values until a perfect matching cannot be found. Deciding whether the graph has a perfect matching can be solved in polynomial time by finding the cardinality of the maximum matching with the Hopcraft-Karp algorithm [13]. We search over a broad range of fixed data qubit layouts to find the conditions that give the smallest communication distances given in Table I. A description of how the data qubit layouts in the search were generated can be found in the supplemental materials [11]. We see that this procedure reduces the maximum communication distance for all codes in Table I and for the $[[144, 12, 12]]$ and $[[288, 12, 18]]$ codes the reduction is almost a factor of three. Four of the five codes after remapping have $D_{\max} \leq 7.21$ which is achievable with Rydberg CZ gates that have been optimized for long distance operation.

There is a large literature on analysis and design of protocols for entangling Rydberg gates [10, 14–18]. It is useful to distinguish between gate errors that arise due to various technical limitations (e.g., laser noise, optical beam pointing, atom motion and position variations at finite temperature, electric and magnetic field noise) and fundamental limits set by atomic structure and quantum physics. Ignoring technical limitations, the entanglement

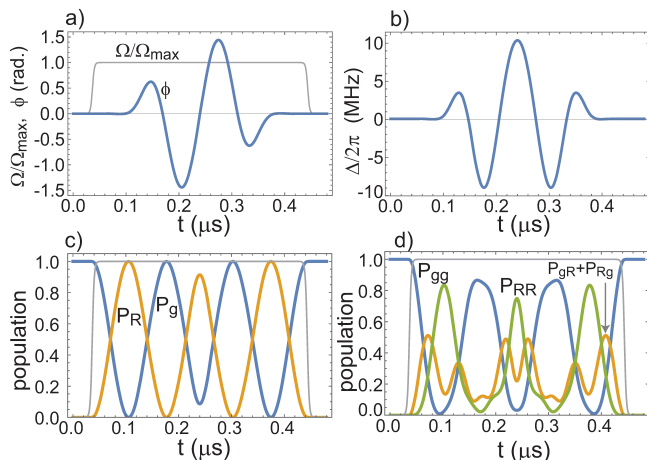


FIG. 3. Rydberg gate simulation at low interaction strength $V/(2\pi) = 3.8$ MHz and Rydberg lifetime 252 ns, corresponding to Cs $90s_{1/2}$ giving error $\epsilon = 7. \times 10^{-4}$. Panels show (a) Rabi drive and phase profile, (b) corresponding detuning, (c) ground P_g and Rydberg P_R populations for one atom coupled to the Rydberg state, and (d) ground P_{gg} , singly excited $P_{gR}+P_{Rg}$ and double Rydberg P_{RR} populations for two atoms coupled to the Rydberg state. Gate parameters are given in row 17 of Table S2 in [11].

fidelity \mathcal{F} of a Rydberg-mediated CZ gate is fundamentally limited by

$$\mathcal{F}_{\max} \leq 1 - \frac{2}{V\tau_R} \quad \text{or} \quad \epsilon_{\min} = 1 - \mathcal{F}_{\max} = \frac{2}{V\tau_R}, \quad (1)$$

where ϵ_{\min} is the minimum gate error, V is the interaction strength between two Rydberg excited atoms, and τ_R is the Rydberg radiative lifetime. This limit follows from the analysis in Ref. [19], and governs the fidelity that can be achieved when two particles interact via states with finite lifetimes. This limit is independent of the specific laser pulse protocol that is used to implement an entangling gate, and thus provides a benchmark to compare entanglement protocols against.

Recent progress in high fidelity Rydberg gates leading to fidelities of $\mathcal{F} > 0.99$ [20–22] has relied on a time optimal protocol that uses a single shaped pulse addressing both atoms [10, 23, 24]. With correct design of the pulse shape, the gate error is dominated by the amount of Rydberg scattering which can be written as $\epsilon_R = T_R/\tau_R$, where T_R is the integrated Rydberg population during the gate and τ_R is the Rydberg state lifetime. In [10] gate designs were presented with an integrated Rydberg population during the gate of $T_R = 2.95/\Omega$ for infinite V and $T_R = 7.6/\Omega$ for $|V/\Omega| = 10$, with Ω the ground-Rydberg Rabi frequency. The solution with finite V gives a gate error of $\epsilon = \epsilon_R = \frac{7.6}{\Omega\tau_R} = \frac{7.6}{V\tau_R}$. Other gate designs [25] have reached $\epsilon = \frac{37.5}{V\tau_R}$, which is also far from the fundamental limit of Eq. (1).

We have improved upon this limit reaching $\epsilon = \frac{4.2}{V\tau_R}$, a factor of 2.1 from the fundamental limit, using an analytical pulse shape as shown in Fig. 3. The Rabi pulse

has constant amplitude with smooth turn on and turn off edges. The phase profile of the pulse is

$$\phi(t) = \Delta_0 t + a \sin[2\pi f(t - t_0)]e^{-[(t-t_0)/\tau]^4} \quad (2)$$

with Δ_0 the detuning from ground-Rydberg resonance, a the amplitude of the phase modulation, f the modulation frequency, t_0 the midpoint of the pulse, and τ providing an envelope width. This phase profile is similar to that in Ref. [20], with the addition of the super-Gaussian envelope and enforcing of anti-symmetry of the phase about the pulse midpoint. The numerical simulation in Fig. 3 accounting for Rydberg decay, but not including any of the technical noise sources enumerated above, verifies that $\mathcal{F} > 0.999$ can be achieved with a relatively small interaction strength of 3.8 MHz and a Rydberg lifetime of $\tau_R = 252$ (μs), which corresponds to the Cs $90s_{1/2}$ state in a room temperature environment. Details of the simulation methodology and calculation of the fidelity are given in Ref. [11]. Further optimization of the gate performance is possible with numerical optimization starting from the analytical pulse shapes used for Table II. An example included in Ref. [11] reaches $\epsilon = \frac{3.9}{V\tau_R}$, less than a factor of two from the fundamental limit.

We note that the Rabi frequency used in Fig. 3 is similar to that which provided an experimental fidelity of 0.995 in Ref. [20], but the interaction strength is more than 100 times smaller. This reduction in interaction strength is significant because it enables a large increase in two-atom separation. With the Cs $90s_{1/2}$ state an interaction strength of $V/(2\pi) = 3.8$ (MHz) is reached at $R_{\max} = 12.3$ (μm) which implies a bicycle code with communication distance of $D = 7.21$ can be implemented with an array of atoms spaced by $s = 1.7$ (μm).

We turn now to estimation of the time needed for each QEC cycle. This estimate depends crucially on the concurrency of the syndrome check operations. While neutral atom architectures support long-range qubit interactions, which are critical for qLDPC bicycle codes, the long-range nature of the Rydberg interaction limits the concurrency, forcing us to execute only one two-qubit gate at a time within a geometrical exclusion zone [26]. At long range, the interaction strength decays as $V(R) \sim 1/R^6$ [27]. Taking the minimum allowed interatomic distance to be R_{\min} for simultaneous check operations of distance R , and the allowed interaction strength to be x we have $R_{\min} = R/x^{1/6}$. Putting $x = 10^{-3}$ we find $R_{\min} = 3.2R$. The [[144, 12, 12]] code uses 288 qubits laid out on a 12×24 grid with a corner to corner distance of 26.8 lattice units. The remapping procedure leads to 17 different check operator distances, each of which occurs the number of times shown in Table II. In order to increase the concurrency, and reduce the cycle time the shorter range gate operations are implemented with lower Rydberg levels that have a smaller exclusion distance.

We estimate the time needed for a full cycle of 864 check operations for the $[[144, 12, 12]]$ code using the distances and gate times in Table II. To avoid incurring additional control system complexity we assume that only one row, corresponding to different gate parameters, can be performed in a single clock cycle. Given the above exclusion zone constraint, the 460 checks in rows 10-17 must be performed one at a time for our layout. For rows 1-9, the 404 operations can be at least partially parallelized, allowing for a reduction to 204 cycles giving a total of 664 clock cycles. Details for achieving this reduction are given in [11]. Accounting for this reduction the effective average gate time is $\langle t_{\text{gate}} \rangle \simeq 0.35 \mu\text{s}$. The single qubit Hadamard operations needed for implementing CNOT gates can be parallelized with microwave control fields and add negligible cycle time. In addition, we allow for a switching time between optical beam configurations of $1.5 \mu\text{s}$ based on proposed architectures for fast photonic beam patterning [28–30], which leads to a cycle time for a full set of X and Z check operations of $664 \times 1.85 \mu\text{s} = 1.2 \text{ ms}$. This value is strongly dependent on assumptions about the optical control system and reconfiguration speed, and could be reduced by multiplexing multiple spatial light modulators, at the cost of additional system complexity. We anticipate that the requisite optical technology will continue to advance and lead to faster execution times, whereas atom transport cannot be accelerated to arbitrary speeds given quantum speed limits for trapped atoms [6].

In addition to a fast rate of syndrome extraction operations, a fast QEC cycle requires fast measurements. State measurements of arrays of neutral atom qubits are most often performed by analysis of fluorescence images acquired by illuminating the atoms with light that resonantly couples one of the qubit states to a short lived excited state, while the other qubit state is sufficiently far detuned to be dark to the imaging light. If the excited state has lifetime τ , photons can be scattered at a maximum rate of $r = 1/(2\tau)$. The rate of detected photons is $r_{\text{det}} = \eta r$ where η accounts for the solid angle of the imaging optics, losses in optical components, and detector quantum efficiency. Typical values for optimized alkali atom experiments are $\tau \sim 30 \text{ ns}$ and $\eta = 0.1$ which leads to a detection rate that could reach $r_{\text{det}} > 1 \times 10^6 \text{ s}^{-1}$.

Neglecting detector noise a state measurement can be based on detection of a single photon, such that sub- μs measurements are in principle possible. In practice, the maximum scattering rate is not used since it leads to excessive atom heating and detector noise necessitates longer integration times, such that state measurements typically require several ms [31], although measurements as fast as 0.5 ms have been reported in free space [5]. Measurement times can be reduced further using more sophisticated image analysis [32] and recently atom occupancy measurements with integration times as short as 2.4 μs have been achieved [33]. While demonstration of

TABLE II. Distribution of communication distances D in units of lattice spacing for the 864 check operations in the $[[144, 12, 12]]$ code. The interaction strength is given at $R = 1.7D$ (μm). The lifetimes of the Rydberg levels are $\tau_{\text{R}} = 60.4, 209, 252$ (μs) for $n = 50, 83, 90$. Details of the Rydberg gate parameters are given in [11].

gate	distance D	occurrences	level	interaction $\frac{V(R)}{2\pi}$ (MHz)	fidelity \mathcal{F}	t_{gate} (ns)
1	1	80	$50s_{1/2}$	415.	0.9996	130
2	1.41	4	$50s_{1/2}$	58.5	0.9993	180
3	2	88	$83s_{1/2}$	1160.	0.9999	150
4	2.24	16	$83s_{1/2}$	780.	0.9999	150
5	3.16	12	$83s_{1/2}$	170.	0.9998	180
6	3.61	12	$83s_{1/2}$	85.	0.9998	180
7	4.12	56	$83s_{1/2}$	40.	0.9998	180
8	4.47	112	$83s_{1/2}$	25.	0.9998	200
9	5	24	$83s_{1/2}$	13.	0.9997	200
10	5.10	4	$83s_{1/2}$	11.5	0.9996	200
11	5.83	8	$83s_{1/2}$	5.2	0.9994	270
12	6	112	$90s_{1/2}$	11.2	0.9996	350
13	6.08	48	$90s_{1/2}$	10.1	0.9995	355
14	6.40	16	$90s_{1/2}$	7.7	0.9994	430
15	6.71	52	$90s_{1/2}$	5.8	0.9994	440
16	7.07	4	$90s_{1/2}$	4.25	0.9993	480
17	7.21	216	$90s_{1/2}$	3.8	0.9993	480

state measurements in large arrays at few μs timescales is an outstanding challenge, we anticipate this will be achieved, such that the time needed for syndrome check operations remains the limiting factor for fast QEC operation.

In summary, we have presented an implementation of qLDPC bivariate bicycle codes based on long range Rydberg gates, which has the potential for reducing the QEC cycle time by an order of magnitude compared to an architecture based on atom transport. The achievable cycle time is critically dependent on the availability of fast photonic beam switching, and improved optical devices will enable further time reductions.

This material is based upon work supported by the U.S. Department of Energy Office of Science National Quantum Information Science Research Centers as part of the Q-NEXT center, as well as support from NSF Award PHY-1720220 and NSF award 2016136 for the QLCI center Hybrid Quantum Architectures and Networks.

While completing this manuscript we became aware of related work on implementation of qLDPC hypergraph codes using Rydberg gates [34].

-
- [1] S. Bravyi, A. W. Cross, J. M. Gambetta, D. Maslov, P. Rall, and T. J. Yoder, High-threshold and low-overhead fault-tolerant quantum memory, *Nature* **627**, 778 (2024).
- [2] A. G. Fowler, M. Mariantoni, J. M. Martinis, and A. N. Cleland, Surface codes: Towards practical large-scale quantum computation, *Phys. Rev. A* **86**, 032324 (2012).
- [3] S. Bravyi, D. Poulin, and B. Terhal, Tradeoffs for reliable quantum information storage in 2D systems, *Phys. Rev. Lett.* **104**, 050503 (2010).
- [4] J. Vizslai, W. Yang, S. F. Lin, J. Liu, N. Nottingham, J. M. Baker, and F. T. Chong, Matching generalized-bicycle codes to neutral atoms for low-overhead fault-tolerance, arXiv:2311.16980 (2023).
- [5] D. Bluvstein, S. J. Evered, A. A. Geim, S. H. Li, H. Zhou, T. Manovitz, S. Ebadi, M. Cain, M. Kalinowski, D. Hangleiter, J. P. Ataides, N. Maskara, I. Cong, X. Gao, P. S. Rodriguez, T. Karolyshyn, G. Semeghini, M. Greiner, V. Vuletić, and M. D. Lukin, Logical quantum processor based on reconfigurable atom arrays, *Nature* **626**, 58 (2024).
- [6] M. R. Lam, N. Peter, T. Groh, W. Alt, C. Robens, D. Meschede, A. Negretti, S. Montangero, T. Calarco, and A. Alberti, Demonstration of quantum brachistochrones between distant states of an atom, *Phys. Rev. X* **11**, 011035 (2021).
- [7] Q. Xu, J. Ataides, C. A. Pattison, N. Raveendran, D. Bluvstein, J. Wurtz, B. Vasic, M. D. Lukin, L. Jiang, and H. Zhou, Constant-overhead fault-tolerant quantum computation with reconfigurable atom arrays, arXiv:2308.08648 (2023).
- [8] M. E. Beverland, P. Murali, M. Troyer, K. M. Svore, T. Hoeffler, V. Kliuchnikov, G. H. Low, M. Soeken, A. Sundaram, and A. Vaschillo, Assessing requirements to scale to practical quantum advantage, arXiv:2211.07629 (2022).
- [9] T. M. Graham, Y. Song, J. Scott, C. Poole, L. Phuttitarn, K. Jooya, P. Eichler, X. Jiang, A. Marra, B. Grinckemeyer, M. Kwon, M. Ebert, J. Cherek, M. T. Lichtman, M. Gillette, J. Gilbert, D. Bowman, T. Ballance, C. Campbell, E. D. Dahl, O. Crawford, N. S. Blunt, B. Rogers, T. Noel, and M. Saffman, Multi-qubit entanglement and algorithms on a neutral-atom quantum computer, *Nature* **604**, 457 (2022).
- [10] S. Jandura and G. Pupillo, Time-optimal two- and three-qubit gates for Rydberg atoms, *Quantum* **6**, 712 (2022).
- [11] See Supplemental Material at [URL will be inserted by publisher] which includes references [35–40].
- [12] (2023), Edward Dahl, private communication.
- [13] J. E. Hopcroft and R. M. Karp, An $n^{5/2}$ algorithm for maximum matchings in bipartite graphs, *SIAM J. Comp.* **2**, 225 (1973).
- [14] D. Jaksch, J. I. Cirac, P. Zoller, S. L. Rolston, R. Côté, and M. D. Lukin, Fast quantum gates for neutral atoms, *Phys. Rev. Lett.* **85**, 2208 (2000).
- [15] M. Saffman, T. G. Walker, and K. Mølmer, Quantum information with Rydberg atoms, *Rev. Mod. Phys.* **82**, 2313 (2010).
- [16] X. L. Zhang, A. T. Gill, L. Isenhower, T. G. Walker, and M. Saffman, Fidelity of a Rydberg blockade quantum gate from simulated quantum process tomography, *Phys. Rev. A* **85**, 042310 (2012).
- [17] H. Levine, A. Keesling, G. Semeghini, A. Omran, T. T. Wang, S. Ebadi, H. Bernien, M. Greiner, V. Vuletić, H. Pichler, and M. D. Lukin, Parallel implementation of high-fidelity multiqubit gates with neutral atoms, *Phys. Rev. Lett.* **123**, 170503 (2019).
- [18] F. Robicheaux, T. Graham, and M. Saffman, Photon recoil and laser focusing limits to Rydberg gate fidelity, *Phys. Rev. A* **103**, 022424 (2021).
- [19] J. H. Wesenberg, K. Mølmer, L. Rippe, and S. Kröll, Scalable designs for quantum computing with rare-earth-ion-doped crystals, *Phys. Rev. A* **75**, 012304 (2007).
- [20] S. J. Evered, D. Bluvstein, M. Kalinowski, S. Ebadi, T. Manovitz, H. Zhou, S. H. Li, A. A. Geim, T. T. Wang, N. Maskara, H. Levine, G. Semeghini, M. Greiner, V. Vuletić, and M. D. Lukin, High-fidelity parallel entangling gates on a neutral-atom quantum computer, *Nature* **622**, 268 (2023).
- [21] S. Ma, G. Liu, P. Peng, B. Zhang, S. Jandura, J. Claes, A. P. Burgers, G. Pupillo, S. Puri, and J. D. Thompson, High-fidelity gates and mid-circuit erasure conversion in an atomic qubit, *Nature* **622**, 279 (2023).
- [22] R. Finkelstein, R. B.-S. Tsai, X. Sun, P. Scholl, S. Direkci, T. Gefen, J. Choi, A. L. Shaw, and M. Endres, Universal quantum operations and ancilla-based readout for tweezer clocks, arXiv: 2402.16220 (2024).
- [23] A. Pagano, S. Weber, D. Jaschke, T. Pfau, F. Meinert, S. Montangero, and H. P. Büchler, Error budgeting for a controlled-phase gate with Strontium-88 Rydberg atoms, *Phys. Rev. Res.* **4**, 033019 (2022).
- [24] M. Mohan, R. de Keijzer, and S. Kokkelmans, Robust control and optimal Rydberg states for neutral atom two-qubit gates, *Phys. Rev. Res.* **5**, 033052 (2023).
- [25] D. Petrosyan, F. Motzoi, M. Saffman, and K. Mølmer, High-fidelity Rydberg quantum gate via a two-atom dark state, *Phys. Rev. A* **96**, 042306 (2017).
- [26] J. M. Baker, A. Litteken, C. Duckering, H. Hoffmann, H. Bernien, and F. T. Chong, Exploiting long-distance interactions and tolerating atom loss in neutral atom quantum architectures, in *2021 ACM/IEEE 48th Annual International Symposium on Computer Architecture (ISCA)* (2021) pp. 818–831.
- [27] T. G. Walker and M. Saffman, Consequences of Zeeman degeneracy for the van der Waals blockade between Rydberg atoms, *Phys. Rev. A* **77**, 032723 (2008).
- [28] T. M. Graham, E. Oh, and M. Saffman, Multi-scale architecture for fast optical addressing and control of large scale qubit arrays, *Appl. Opt.* **62**, 3242 (2023).
- [29] A. J. Menssen, A. Hermans, I. Christen, T. Propson, C. Li, A. J. Leenheer, M. Zimmermann, M. Dong, H. Larocque, H. Raniwala, G. Gilbert, M. Eichenfield, and D. R. Englund, Scalable photonic integrated circuits for high-fidelity light control, *Optica* **10**, 1366 (2023).
- [30] B. Zhang, P. Peng, A. Paul, and J. D. Thompson, Scaled local gate controller for optically addressed qubits, *Optica* **11**, 227 (2024).
- [31] T. M. Graham, L. Phuttitarn, R. Chinnarasu, Y. Song, C. Poole, K. Jooya, J. Scott, A. Scott, P. Eichler, and M. Saffman, Mid-circuit measurements on a neutral atom quantum processor, *Phys. Rev. X* **13**, 041051 (2023).
- [32] L. Phuttitarn, B. M. Becker, R. Chinnarasu, T. M. Graham, and M. Saffman, Enhanced measurement of neutral atom qubits with machine learning, arXiv:2311.12217 (2023).

- [33] L. Su, A. Douglas, M. Szurek, A. H. Hebert, A. Krahn, R. Groth, G. A. Phelps, O. Markovic, and M. Greiner, Fast single atom imaging in optical lattice arrays, arXiv:2404.09978 (2024).
- [34] L. Pecorari, S. Jandura, G. K. Brennen, and G. Pupillo, High-rate quantum LDPC codes for long-range-connected neutral atom registers, arXiv:2404.13010 (2024).
- [35] L. H. Pedersen, N. M. Møller, and K. Mølmer, Fidelity of quantum operations, *Phys. Lett. A* **367**, 47 (2007).
- [36] M. Saffman, I. I. Beterov, A. Dalal, E. J. Paez, and B. C. Sanders, Symmetric Rydberg controlled- Z gates with adiabatic pulses, *Phys. Rev. A* **101**, 062309 (2020).
- [37] S. Jandura, J. D. Thompson, and G. Pupillo, Optimizing Rydberg gates for logical-qubit performance, *PRX Quantum* **4**, 020336 (2023).
- [38] C. Fromonteil, D. Bluvstein, and H. Pichler, Protocols for Rydberg entangling gates featuring robustness against quasistatic errors, *PRX Quantum* **4**, 020335 (2023).
- [39] W.-X. Li, J.-L. Wu, S.-L. Su, and J. Qian, High-tolerance antiblockade SWAP gates using optimal pulse drivings, *Phys. Rev. A* **109**, 012608 (2024).
- [40] N. Khaneja, T. Reiss, C. Kehlet, T. Schulte-Herbrüggen, and S. J. Glaser, Optimal control of coupled spin dynamics: design of NMR pulse sequences by gradient ascent algorithms, *J. Mag. Res.* **172**, 296 (2005).

Supplemental material for Architecture for fast implementation of qLDPC codes with optimized Rydberg gates

C. Poole,¹ T. M. Graham,¹ M. A. Perlin,² M. Otten,¹ and M. Saffman^{1,3}

¹*Department of Physics, University of Wisconsin-Madison, 1150 University Avenue, Madison, WI, 53706 USA*

²*Inflection, Inc., Chicago, IL, 60615, USA*

³*Inflection, Inc., Madison, WI, 53703, USA*

(Dated: April 30, 2024)

This document contains additional information concerning the procedure for optimizing the qubit layout, CZ fidelity calculation, simulations of Rydberg gate fidelity, gate parameters, and concurrency of gate operations.

CONTENTS

I. Optimizing the qubit layout	1
II. Gate fidelity	2
III. Analytical gate parameters	4
IV. Concurrency of gate operations	5
V. Numerically optimized gates	6
References	6

I. OPTIMIZING THE QUBIT LAYOUT

The bivariate bicycle qLDPC codes are constructed in the following manner [S1]. Let S_ℓ be the cyclic shift matrix of dimension $\ell \times \ell$. Row i of S_ℓ has a single nonzero entry equal to one at column $i + 1 \pmod{\ell}$. For example,

$$S_3 = \begin{bmatrix} 0 & 1 & 0 \\ 0 & 0 & 1 \\ 1 & 0 & 0 \end{bmatrix}.$$

Note also that S_ℓ^ℓ has order ℓ , $S_\ell^\ell = I_\ell$ the $\ell \times \ell$ identity matrix. We can define polynomials

$$x^p y^q = S_\ell^p \otimes S_m^q \quad (\text{S1})$$

with $0 \leq p < \ell$, $0 \leq q < m$. A bivariate bicycle code is defined by a pair of matrices

$$A = A_1 + A_2 + A_3 \text{ and } B = B_1 + B_2 + B_3 \quad (\text{S2})$$

where each term A_i and B_j is a power of x or y [S1]. The check matrices for the code are given by

$$H^X = [A|B] \text{ and } H^Z = [B^T|A^T]. \quad (\text{S3})$$

As an explicit example, with $\ell = 12$ and $m = 6$, the matrices $A = x^3 + y + y^2$ and $B = y^3 + x + x^2$ result in the $[[144,12,12]]$ code from Ref. [S1]. In this way, an X check represented by row i involves a data qubit represented by column j if $H_{ij}^X = 1$, and likewise for Z checks and H^Z . We follow the labelling convention from Ref. [S1] by partitioning the data qubits into two sets L and R given by the left and right blocks of columns in the check matrices, respectively. This gives four sets of qubits L , R , X , and Z , each of size $n/2 = \ell m$, which we may assign integer labels from $\mathbb{Z}_{\ell m} = \{0, 1, \dots, \ell m - 1\}$. Data qubits and checks may equivalently be labeled by monomials from $\mathcal{M} = \{1, y, \dots, y^{m-1}, x, xy, \dots, xy^{m-1}, \dots, x^{\ell-1}y^{m-1}\}$ so that a qubit with label $i \in \mathbb{Z}_{\ell m}$ may alternatively

TABLE S1. Bivariate bicycle codes with n data qubits, $2n$ total qubits (including ancillae), k logical qubits, and code distance d . For each code, we provide the parameters defining the code [S1], the monomials used to generate the optimal layout, and the maximum communication distance D_{\max} in units of the lattice spacing using our method.

$[[n, k, d]]$	ℓ, m	A	B	L_1	L_2	R_1	R_2	LR	D_{\max}
$[[72, 12, 6]]$	6, 6	$x^3 + y + y^2$	$y^3 + x + x^2$	x^2y	x^5y^5	x^4y^5	xy	x^3	5.
$[[90, 8, 10]]$	15, 3	$x^9 + y + y^2$	$1 + x^2 + x^7$	x^5	x^9y	x^{10}	x^6y^2	x	10.
$[[108, 8, 10]]$	9, 6	$x^3 + y + y^2$	$y^3 + x + x^2$	x^3y	x^7y^2	x^3xy	x^2y^4	x^5	7.
$[[144, 12, 12]]$	12, 6	$x^3 + y + y^2$	$y^3 + x + x^2$	x^2y^3	$x^{11}y^4$	x^2y^3	$x^{11}y^4$	y^2	7.21
$[[288, 12, 18]]$	12, 12	$x^3 + y^2 + y^7$	$y^3 + x + x^2$	y^7	xy^9	y^7	xy^9	y^6	7.21

be labelled by $x^{a_i}y^{i-ma_i}$ for $a_i = \text{floor}(i/m)$ [S1]. Our goal is to assign each qubit a position on a grid with open boundary conditions such that the distance D_{\max} of the longest range check operation is minimized.

A brute force search of all possible layouts is not feasible due to the combinatorially large number of possibilities. Instead, we perform a limited search over initial position assignments for the L and R data qubits, and for each initial layout we solve for the assignment of the ancilla X and Z qubit positions which minimizes the distance D_{\max} of the longest range check operation. Note that the set \mathcal{M} together with polynomial multiplication forms an abelian group isomorphic to $\mathbb{Z}_\ell \times \mathbb{Z}_m$. We seek a one to one mapping of elements from this group onto a rectangular grid. The mapping we use is defined by five monomials $L_1, L_2, R_1, R_2, LR \in \mathcal{M}$. For the mapping to be well defined, L_1 and L_2 must satisfy conditions of lemma 4 from Ref. [S1] to obtain a well defined enumeration of the L qubits:

- (i) $\langle L_1, L_2 \rangle = \mathcal{M}$ and
- (ii) $\text{ord}(L_1)\text{ord}(L_2) = \ell m$.

Here, $\langle L_1, L_2 \rangle$ is the group generated by the subset $\{L_1, L_2\}$ and $\text{ord}(\alpha)$ is the order of α , the smallest positive integer p such that $\alpha^p = 1$. R_1 and R_2 must also satisfy these conditions, with the additional constraint that $\text{ord}(R_1) = \text{ord}(L_1)$ and $\text{ord}(R_2) = \text{ord}(L_2)$. Letting $\mu = \text{ord}(L_1)$ and $\lambda = \text{ord}(L_2)$, we construct a $2\mu \times 2\lambda$ grid of qubits. For each L qubit with label $\alpha_L \in \mathcal{M}$, there is a unique $(a, b) \in \mathbb{Z}_\mu \times \mathbb{Z}_\lambda$ such that $\alpha_L = L_1^a L_2^b$. We initially assign qubit L with label α_L to the grid position $(2a, 2b)$. Likewise, there is a unique $(a, b) \in \mathbb{Z}_\mu \times \mathbb{Z}_\lambda$ such that $\alpha_R = LR(R_1^a R_2^b)$ and initially assign data qubit R with label α_R to grid position $(2a + 1, 2b + 1)$. The layout of data qubits from [S1] and [S2] may be reproduced as special cases by the appropriate choice of five monomials. In [S1], monomials $A_i, A_j^T, B_g,$ and B_h^T are selected from the monomial terms that produce the code to form $L_1 = R_1 = A_i A_j^T, L_2 = R_2 = B_g B_h^T, LR = A_j^T B_g$. By selecting the monomials in this way, they produce a ‘toric’ layout where, if the grid is considered to have periodic boundary conditions, four of the six connections for each qubit are nearest neighbor interactions. To produce the layout of [S2], take $L_1 = R_1 = y, L_2 = R_2 = x, LR = 1$, which directly enumerates the qubits in a column-major order.

We search over all possible values of L_1 and L_2 which satisfy the above conditions. For the smaller codes ($n < 144$), we also searched over all values of R_1 and R_2 , but found that the best result consistently had $R_{1(2)} \in \{L_{1(2)}, L_{1(2)}^T\}$. Thus, we limit the search for larger codes to this range. Lastly, we let $LR \in \mathcal{M}$ be arbitrary. After initially placing each of the L and R qubits, the entire grid is remapped according to the plane ‘folding’ procedure illustrated in Fig. 2 in the main text. At this stage, the positions of L and R qubits are considered fixed, and we must identify an assignment of X and Z qubits which minimizes the maximum check operator distance D_{\max} . This is done using a bipartite matching procedure as explained in the main text.

As an example the layout of the $[[144, 12, 12]]$ code after optimization to achieve $D_{\max} = 7.21$ is given in Fig. S1. A table enumerating the monomials that produce the best layouts found for each code is given in Table S1.

II. GATE FIDELITY

Consider a generalized diagonal gate U_d that results in the unitary evolution

$$\begin{aligned}
 |00\rangle &\rightarrow U_d |00\rangle = a_{00} e^{2\phi_{00}} |00\rangle \\
 |01\rangle &\rightarrow U_d |01\rangle = a_{01} e^{2\phi_{01}} |01\rangle \\
 |10\rangle &\rightarrow U_d |10\rangle = a_{10} e^{2\phi_{10}} |10\rangle \\
 |11\rangle &\rightarrow U_d |11\rangle = a_{11} e^{2\phi_{11}} |11\rangle
 \end{aligned} \tag{S4}$$

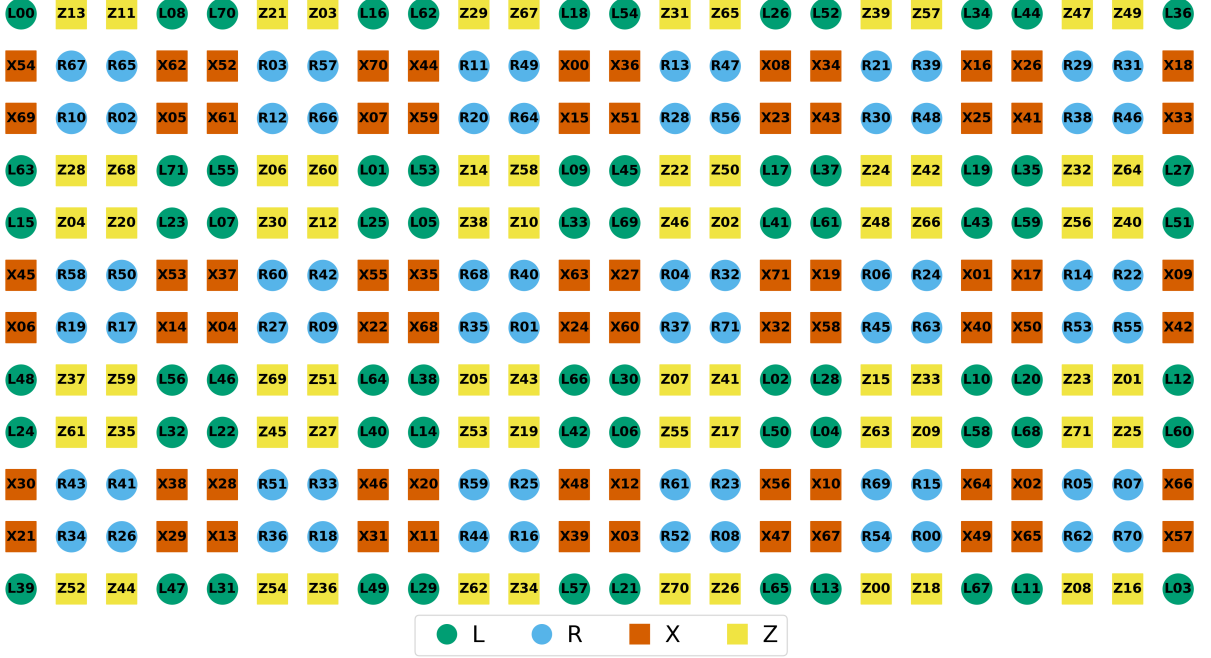


FIG. S1. Optimized layout of the $[[144,12,12]]$ code with a maximum communication distance of 7.21 lattice spacings. All nodes are labeled. Edges can be generated via the rules for the $[[144,12,12]]$ code.

where a_{ij} are real amplitudes and ϕ_{ij} are real phases. A phase gate would have $a_{00} = a_{01} = a_{10} = a_{11} = 1$. Imperfect Rydberg phase gates have the $a_{ij} \leq 1$ due to rotation errors that do not fully return population to the computational basis states.

A Bell state can be prepared with the sequence

$$|\psi\rangle = [I \otimes R_x(\pi/2)][R_z(-\phi_{10}) \otimes R_z(-\phi_{01})]U_d[R_x(\pi/2) \otimes R_x(\pi/2)]|00\rangle. \quad (\text{S5})$$

In the ideal case where $a_{00} = a_{01} = a_{10} = a_{11} = 1$, $\phi_{00} = 0$, and introducing the gate phase $\phi = \phi_{11} - \phi_{01} - \phi_{10}$ the output state is

$$|B\rangle = -ie^{i\frac{\phi_{01} + \phi_{10}}{2}} \frac{|01\rangle + |10\rangle}{\sqrt{2}}$$

when $\phi = \pi$. This is a maximally entangled Bell state up to an irrelevant global phase.

In the phase gate limit with $a_{ij} = 1$ the Bell fidelity of the output state is

$$\mathcal{F}_{\text{pg}} = |\langle B | \psi \rangle|^2 = \frac{3 + 2 \cos(\phi_{00}) - \cos(\phi - \phi_{00}) - 2 \cos(\phi)}{8}. \quad (\text{S6})$$

The Bell fidelity depends on the phase ϕ_{00} . For Rydberg gates that couple state $|1\rangle$ to the Rydberg level off-resonant light shifts are responsible for the phase ϕ_{00} . These shifts can be cancelled by applying a sequence of z and x single qubit rotations. We may therefore set $\phi_{00} = 0$ in which case the fidelity reduces to

$$\mathcal{F}_{\text{pg},0} = \frac{5 - 3 \cos(\phi)}{8}.$$

For realistic Rydberg gates there is also an error contribution due to imperfect rotations that leave population outside the qubit basis. To analyze the fidelity in this situation we can work in a three dimensional basis $\{|0\rangle, |1\rangle, |r\rangle\}$, with $|r\rangle$ the Rydberg state. Tracing over the Rydberg state, we have an effective unitary in the qubit basis of the form of eq. (S4).

Assuming $a_{00} = 1$ and a symmetric gate such that $a_{10} = a_{01}$, $\phi_{10} = \phi_{01}$ we find

$$\mathcal{F}_{\text{sym}} = \frac{1 + 4a_{01}^2 + a_{11}^2 + 4a_{01} \cos(\phi_{00}) - 2a_{11} \cos(\phi - \phi_{00}) - 4a_{01}a_{11} \cos(\phi)}{16}.$$

If we again assume $\phi_{00} = 0$ this reduces to

$$\mathcal{F}_{\text{sym},0} = \frac{1 + 4a_{01}^2 + 4a_{01} + a_{11}^2 - 2(1 + 2a_{01})a_{11} \cos(\phi)}{16}. \quad (\text{S7})$$

Equation (S7) gives the fidelity for preparing a Bell state starting from the state $|00\rangle$. We can generalize this to give the fidelity of an operator U with respect to the ideal operator U_0 averaged over all two-qubit initial states. A convenient expression for calculating the average fidelity is [S3]

$$\mathcal{F}_{\text{ave}} = \frac{n + |\text{Tr}(U_0^\dagger U)|^2}{n(n+1)}.$$

where n is the dimension of the Hilbert space and we have used the fact that U_0 and U are unitary. Using $n = 4$,

$$\begin{aligned} U_0 &= \begin{pmatrix} 1 & 0 & 0 & 0 \\ 0 & 1 & 0 & 0 \\ 0 & 0 & 1 & 0 \\ 0 & 0 & 0 & -1 \end{pmatrix}, \\ U &= [\text{R}_z(-\phi_{10}) \otimes \text{R}_z(-\phi_{01})]U_d \\ &= e^{i\frac{\phi_{01} + \phi_{10}}{2}} \begin{pmatrix} a_{00}e^{i\phi_{00}} & 0 & 0 & 0 \\ 0 & a_{01} & 0 & 0 \\ 0 & 0 & a_{10} & 0 \\ 0 & 0 & 0 & a_{11}e^{i\phi} \end{pmatrix} \end{aligned} \quad (\text{S8})$$

and assuming $a_{00} = 1, \phi_{00} = 0$ with the symmetric conditions $a_{10} = a_{01}, \phi_{10} = \phi_{01}$, we find

$$\mathcal{F}_{\text{ave}} = \frac{5 + 4a_{01}^2 + 4a_{01} + a_{11}^2 - 2(1 + 2a_{01})a_{11} \cos(\phi)}{20}. \quad (\text{S9})$$

The average fidelity \mathcal{F}_{ave} was found by simulating the coherent evolution using the gate and interaction parameters from Table S2 by numerical solution of the Schrödinger equation and extracting the values of a_{01}, a_{11} , and ϕ . The fidelity reported in the main text and in Table S2 was corrected for Rydberg state decay using

$$\mathcal{F} = \mathcal{F}_{\text{ave}} - T_{\text{R}}/\tau_{\text{R}} \quad (\text{S10})$$

where τ_{R} is the Rydberg lifetime and the integrated Rydberg population averaged over the computational basis states is

$$T_{\text{R}} = \frac{1}{2} \int_0^{t_{\text{gate}}} dt |c_{\text{R}}(t)|^2 + |c_{\text{gR}}(t)|^2 + |c_{\text{RR}}(t)|^2.$$

Here $c_{\text{R}}(t)$ is the Rydberg amplitude when one atom is Rydberg coupled, $c_{\text{gR}}(t)$ is the amplitude of the singly occupied Rydberg state when two atoms are Rydberg coupled, and $c_{\text{RR}}(t)$ is the amplitude of the doubly occupied Rydberg state. All calculations assumed symmetrical behavior of the two atoms.

III. ANALYTICAL GATE PARAMETERS

The analytical pulses are based on a constant amplitude Rabi drive with smooth turn on and turn off and a modulated phase profile. The Rabi amplitude is given by

$$\Omega(t) = \Omega_0 \left[\frac{1}{1 + e^{-(t-20\tau_e)/\tau_e}} + \frac{1}{1 + e^{-(t_{\text{gate}}-20\tau_e-t)/\tau_e}} - 1 \right] \quad (\text{S11})$$

with $\tau_e = 1.825$ ns and t_{gate} the nominal gate duration. The phase profile is

$$\phi(t) = \Delta_0 t + a \sin[2\pi f(t - t_0)]e^{-[(t-t_0)/\tau]^4} \quad (\text{S12})$$

TABLE S2. Gate parameters and performance for the Euclidean communication distances D in units of lattice spacing for the 864 check operations in the $[[144, 12, 12]]$ code. The interaction strength is given at $R = 1.7D$ (μm). The lifetimes of the Rydberg levels are $\tau_R = 60.4, 209, 252$ (μs) for $n = 50, 83, 90$.

gate	lattice distance D	connection R (μm)	Rydberg level	interaction $V(R)/2\pi$ (MHz)	fidelity \mathcal{F}	t_{gate} (ns)	a	f (MHz)	$\Omega/2\pi$ (MHz)	$\Delta_0/2\pi$ (MHz)	τ (ns)	V/Ω	$\epsilon/\epsilon_{\text{min}}$
1	1	1.7	$50s_{1/2}$	415.	0.9996	130	0.774	20.0	21.5	-1.59	1907	19.3	31.
2	1.41	2.40	$50s_{1/2}$	58.5	0.9993	180	0.749	10.6	11.3	-1.59	374	5.2	7.8
3	2.0	3.4	$83s_{1/2}$	1160.	0.9999	150	1.44	9.96	15.9	-0.818	20	73.	76.
4	2.24	3.81	$83s_{1/2}$	780.	0.9999	150	1.45	9.91	15.9	-0.856	20	49.	51.
5	3.16	5.37	$83s_{1/2}$	170.	0.9998	180	0.707	11.5	11.4	-0.451	744	15.	22.
6	3.61	6.14	$83s_{1/2}$	85.	0.9998	180	0.594	13.3	11.2	0.152	922	7.6	11.
7	4.12	7.00	$83s_{1/2}$	40.	0.9998	180	0.569	14.1	11.1	-0.505	81	3.6	5.3
8	4.47	7.60	$83s_{1/2}$	25.	0.9998	200	0.622	14.4	9.54	-0.897	452	2.6	3.3
9	5	8.65	$83s_{1/2}$	13.	0.9997	200	1.10	15.6	19.6	1.52	2000	0.66	2.6
10	5.10	8.67	$83s_{1/2}$	11.5	0.9996	200	2	13.0	25.5	0.312	1347	0.45	3.0
11	5.83	9.91	$83s_{1/2}$	5.2	0.9994	270	2	14.6	22.9	1.22	115	0.23	2.0
12	6	10.2	$90s_{1/2}$	11.2	0.9996	350	0.578	6.42	4.32	-0.383	1756	2.6	3.5
13	6.08	10.3	$90s_{1/2}$	10.1	0.9995	355	1.68	11.0	10.0	0.649	203	1.0	4.0
14	6.40	10.9	$90s_{1/2}$	7.7	0.9994	430	1.74	8.00	8.84	0.260	164	0.87	3.7
15	6.71	11.4	$90s_{1/2}$	5.8	0.9994	440	1.50	8.13	8.41	0.315	264	0.69	2.8
16	7.07	12.0	$90s_{1/2}$	4.3	0.9993	480	1.46	9.34	6.19	-1.46	1897	0.69	2.4
17	7.21	12.3	$90s_{1/2}$	3.8	0.9993	480	1.46	7.06	7.26	0.074	103	0.52	2.1

with $t_0 = t_{\text{gate}}/2$ the midpoint. The parameters $\Omega_0, \Delta_0, a, f, \tau$ are chosen to optimize the fidelity for given V, τ_R values. Table S2 provides parameters found from numerical search for the analytical Rydberg gate designs used in the main text.

As can be seen in the Table it is possible to choose parameters that provide fidelity $\mathcal{F} \geq 0.9993$ for inter-atomic distances ranging from 1.7 to 12.3 μm . The gate designs have a wide range of parameters with the apodization parameter τ in eq. (S12) being much less than t_{gate} in some case and much larger than t_{gate} in others. When $\tau \gg t_{\text{gate}}$ the phase function reduces to that used in [S4]. None of the gates are in the strong blockade regime with V/Ω ranging from 73. all the way down to 0.52. This implies that each gate must be calibrated for specific inter-atomic distances.

The reported fidelities are for the idealized situation of no additional technical errors due to laser noise, optical beam pointing, atom motion and position variations at finite temperature, or electric and magnetic field noise. Pulse designs that suppress sensitivity to these effects [S5–S9] are important for implementation, but are outside the scope of this work.

IV. CONCURRENCY OF GATE OPERATIONS

Due to the long range nature of the Rydberg interaction only a limited number of gates can be executed in one clock cycle. For the layout in Fig. S1, every check in rows 10-17 of Table S2 interferes with all other checks of the same distance, and thus they must be performed one at a time. For rows 4-9, it is possible to perform at most two check operations concurrently. For rows 2-3, at most four check operations may be performed concurrently. For row 1, at most fourteen may be performed concurrently. For each of these rows, we apply a greedy algorithm which selects a grouping of maximum size to be scheduled. Any other groupings of maximum size that involved qubits in the selected group are removed from consideration, and the process is repeated until every check operation is included in one of the groupings. During this process, the maximum cardinality of remaining groupings may decrease. The specific choice of maximum size grouping to be selected is determined by choosing the option which maximizes the number of remaining groupings. If there are multiple equivalently good options to choose from based on this metric, we may choose at random and repeat this process several times, keeping the best end result. By applying this process for each row, we get a total of $9 + 1 + 24 + 8 + 6 + 6 + 38 + 98 + 14 + 4 + 8 + 112 + 48 + 16 + 52 + 4 + 216 = 664$ clock cycles. This leads to the estimate for a full QEC cycle given in the main text.

We note that the number of clock cycles could be reduced somewhat by introducing additional Rydberg levels such

that the range of the Rydberg interaction is as short as possible consistent with performing a gate of high fidelity at the desired distance.

V. NUMERICALLY OPTIMIZED GATES

The analytical pulse parameters used for Table S2 can be further optimized, in the sense of getting slightly closer to the fundamental limit of ϵ_{\min} , by allowing for the Rabi drive $\Omega(t)$ to have a time dependent value. The example shown in Fig. S2 reaches $\epsilon/\epsilon_{\min} = 1.9$. The amplitude and phase profiles were found using the GRAPE algorithm[S10].

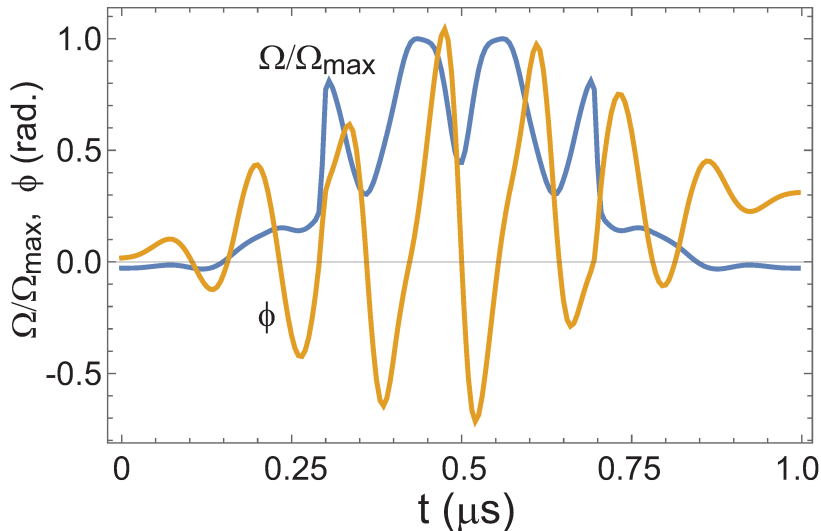


FIG. S2. Single pulse Rydberg CZ gate found numerically with fidelity $\mathcal{F} = 0.9989$. Parameters: $\Omega_{\max}/2\pi = 10.84$ MHz, $V/2\pi = 2.2$ MHz, $\tau_R = 252$ μ s.

-
- [S1] S. Bravyi, A. W. Cross, J. M. Gambetta, D. Maslov, P. Rall, and T. J. Yoder, High-threshold and low-overhead fault-tolerant quantum memory, *Nature* **627**, 778 (2024).
- [S2] J. Viszlai, W. Yang, S. F. Lin, J. Liu, N. Nottingham, J. M. Baker, and F. T. Chong, Matching generalized-bicycle codes to neutral atoms for low-overhead fault-tolerance, arXiv:2311.16980 (2023).
- [S3] L. H. Pedersen, N. M. Møller, and K. Mølmer, Fidelity of quantum operations, *Phys. Lett. A* **367**, 47 (2007).
- [S4] S. J. Evered, D. Bluvstein, M. Kalinowski, S. Ebadi, T. Manovitz, H. Zhou, S. H. Li, A. A. Geim, T. T. Wang, N. Maskara, H. Levine, G. Semeghini, M. Greiner, V. Vuletić, and M. D. Lukin, High-fidelity parallel entangling gates on a neutral-atom quantum computer, *Nature* **622**, 268 (2023).
- [S5] M. Saffman, I. I. Beterov, A. Dalal, E. J. Paez, and B. C. Sanders, Symmetric Rydberg controlled- Z gates with adiabatic pulses, *Phys. Rev. A* **101**, 062309 (2020).
- [S6] M. Mohan, R. de Keijzer, and S. Kokkelmans, Robust control and optimal Rydberg states for neutral atom two-qubit gates, *Phys. Rev. Res.* **5**, 033052 (2023).
- [S7] S. Jandura, J. D. Thompson, and G. Pupillo, Optimizing Rydberg gates for logical-qubit performance, *PRX Quantum* **4**, 020336 (2023).
- [S8] C. Fromonteil, D. Bluvstein, and H. Pichler, Protocols for Rydberg entangling gates featuring robustness against quasistatic errors, *PRX Quantum* **4**, 020335 (2023).
- [S9] W.-X. Li, J.-L. Wu, S.-L. Su, and J. Qian, High-tolerance antiblockade SWAP gates using optimal pulse drivings, *Phys. Rev. A* **109**, 012608 (2024).
- [S10] N. Khaneja, T. Reiss, C. Kehlet, T. Schulte-Herbrüggen, and S. J. Glaser, Optimal control of coupled spin dynamics: design of NMR pulse sequences by gradient ascent algorithms, *J. Mag. Res.* **172**, 296 (2005).